Growth of Fe_3O_4(001) thin films on Pt(100): Tuning surface termination with an Fe buffer layer

Earl M. Davis, Ke Zhang, Yi Cui, Helmut Kuhlenbeck, Shamil Shaikhutdinov,*
Hans-Joachim Freund

Abteilung Chemische Physik, Fritz-Haber-Institut der Max-Planck-Gesellschaft, Faradayweg 4-6, 14195 Berlin, Germany

Abstract. We studied the preparation of well-ordered thin Fe_3O_4(001) films on a metallic substrate, Pt(100), using LEED and STM. The results show that film growth either by Fe reactive deposition in oxygen or by deposition-oxidation cycles onto pure Pt(100) results primarily in (111)-oriented surfaces. To grow Fe_3O_4(001) films, the preparation must include deposition of an Fe buffer layer as previously suggested for the growth of Fe_3O_4(001) on MgO(001) (Spiridis et al. Phys. Rev. B 74 (2006) 155423). Two stable (so called "dimer"- and B-layer) surface terminations were observed, both exhibiting a $(\sqrt{2}\times\sqrt{2})R45^{o}$ reconstruction. Several intermediate, Fe-rich terminations were observed during the annealing process of an initially dimer-like structure. The process critically depends on the thickness of the buffer layer, which can be used as a tuning parameter for surface structures.

*Corresponding author: shaikhutdinov@fhi-berlin.mpg.de

1. Introduction

Iron oxides are one of the most widespread materials on our planet, for example, as iron ores, rust, etc. A number of iron oxide phases exist as naturally grown crystals, FeO (wüstite), Fe_3O_4 (magnetite) and Fe_2O_3 (hematite, maghemite) being the most common. To understand surface structures and chemistry of iron oxides, single crystal surfaces as well as thin films were used as planar model systems, which are well-suited for surface science studies [1-3]. Although oxides on iron metal surfaces are naturally formed as passivating films, these are usually poorly-ordered and exhibit a complex stoichiometry depending on the preparation conditions. Growth of well-ordered iron oxide films has been reported on Pt(111) [3], and to a much lesser extent on other metal substrates [1].

Investigations on the structures of iron oxides have primarily focused on the close–packed surfaces such as Fe_3O_4(111) and Fe_2O_3(0001). Recently, more work has been directed toward the Fe_3O_4(001) surface following expectations of a large difference in reactivity when compared to the (111) surface (see, for example, refs. [4, 5]). In the {001} direction, the layers of tetrahedral iron atoms are denoted as A-layers and the mixed octahedrally coordinated iron and oxygen layers are termed B layers (see Fig. 1a). It is well established that the Fe_3O_4(001) surface exhibits a $(\sqrt{2}\times\sqrt{2})R45^o$ reconstruction [6-8]. This reconstruction was initially discussed in terms of surface charge neutrality as a driving force. Further studies suggested an autocompensated B-layer termination, which consists of a layer of octahedrally coordinated iron and tetrahedrally coordinated oxygen, along with one oxygen vacancy per unit cell [7, 9]. The surface phase diagram constructed in the framework of ab initio thermodynamics revealed that a modified B-layer is stabilized over a broad range of oxygen pressures. Instead of an ordering of surface defects in previously proposed models, the stabilization involves Jahn–Teller distortion with a wavelike displacement of Fe and O atoms in the top B layer, whereby the $(\sqrt{2}\times\sqrt{2})R45^o$ superstructure is formed, as shown in Fig. 1b [10, 11]. Further density functional theory (DFT) studies suggested very close surface energies for A- and B-terminated surfaces, making the observation of these surfaces sensitive to the preparation conditions [12], as indeed observed by Parkinson et al., who showed that both the B-termination and a metastable A-termination can be reproducibly prepared on a single crystal sample within one sputter/anneal cycle through variation of the annealing temperature [13]. The authors also concluded that charge compensation arguments based on nominal bulk charges are unreliable for predicting the

surface structure of magnetite. Very recently, using a combination of quantitative low-energy electron diffraction (LEED), STM, and DFT calculations, Bliem et al. rationalized the (√2×√2)R45° reconstruction in terms of an ordered array of subsurface iron vacancies and interstitials [14].

To better control the surface stoichiometry of the Fe_3O_4(001) films on MgO(001) (commonly used as a substrate due to the low lattice mismatch, ca. 3 %), Korecki and coworkers made use of an ~20 nm-thick Fe(001) film prior to the iron oxide growth [15]. They found that the Fe buffer layer, initially inserted to prevent migration of Mg atoms and to allow higher annealing temperatures, resulted in an Fe-rich termination, termed hereafter as a "dimer" termination (first predicted by molecular dynamics simulations [16]). The atomic structure proposed by Korecki's group, shown in Fig. 1c [17], has been revisited by Diebold, Parkinson and co-workers [13, 18]. They also reported that this termination can be prepared by iron deposition on an initially B-terminated surface. Notably, these two surfaces both exhibit a (√2×√2)R45° reconstruction, making them difficult to distinguish without scanning tunnelling microscopy (STM) imaging.

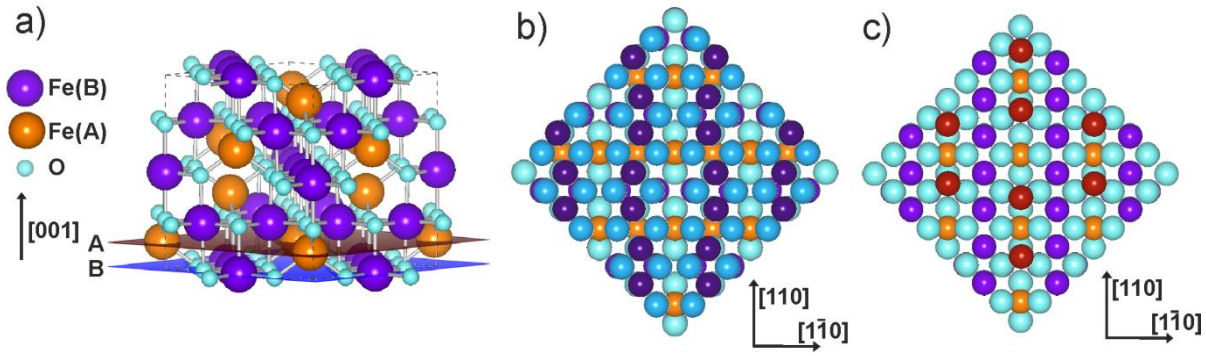

Figure 1. (a) Bulk structure unit cell of Fe_3O_4. (b,c) Top views of Fe_3O_4(100) surface structures as suggested by Pentcheva et al. [10] for the B-terminated surface (b), and by Spiridis et al. [15] for the "dimer"-terminated surface (c). Darker shading indicates atoms in the surface layer.

In continuation of our long-standing studies on surface chemistry of iron oxide films, in this paper we address the growth of thin Fe_3O_4(100) films on a *metallic* substrate. The metal support facilitates using surface science tools, particularly vibrational and electron spectroscopies. To the best of our knowledge, growth of Fe_3O_4(100) on a metal support has

only been mentioned by Fonin et al. [19] for W(100) in the course of the work function measurements, however, detailed surface structure characterisation has not been provided. Since Pt(111) has successfully been used for growth of crystalline Fe_3O_4(111) films, it is near at hand to use Pt(100) as a substrate to grow (100)-oriented films. Note, however, that Ritter et al. [20] have briefly mentioned that the growth of multilayer iron oxide films on both Pt(100) and Pt(111) leads to (111)-exposing surfaces. In this work, we show that well-ordered Fe_3O_4(001) films can successfully be grown on Pt(100) and also show that the two most stable terminations can both be achieved through variation of growth parameters.

2. Materials and Methods

The experiments were carried out in an ultra-high vacuum (UHV) chamber (base pressure 2×10^{-10} mbar) equipped with low energy electron diffraction (LEED) and Auger electron spectroscopy (from Specs) and STM (from Omicron). The clean surface of Pt(100) (from MaTeck) was prepared through cycles of Ar^+-sputtering and UHV annealing until the characteristic "hex"-reconstruction was observed in LEED. Iron was deposited using an e-beam assisted evaporator (EFM 3, Omicron). The deposition rate (~ 7 Å/min) was calibrated by STM in the same way as in ref. [21], where it was shown that Fe atoms on Pt(100) at low coverages undergo atomic site exchange, with Fe atoms preferentially sitting in the sub-surface region and Pt islands forming at the surface.

3. Results and discussion

Since previous studies have shown that preparation of Fe_3O_4 films by cycles of Fe deposition in UHV and oxidation resulted in (111)-oriented films on both Pt(111) and Pt(100) [20, 22], we first examined, for comparison, film growth by Fe deposition in an oxygen ambient ("reactive deposition"), followed by annealing at elevated temperatures to achieve well-ordered films.

Increasing amounts of iron, between 8 and 50 nm, on a Pt(100)-hex surface in 10^{-5} mbar of O_2 at 300 K totally vanish LEED patterns, thus indicating a highly disordered surface. Upon subsequent annealing in UHV at 550 K some diffraction spots start to appear although very diffuse. Basically, the same surface was obtained by reactive deposition directly at 550 K.

Further step-wise annealing to 645 K and then to 775 K, for 60 min each, considerably improves film ordering, as judged by LEED, but resultant surfaces exhibited hexagonal symmetry (Fig. 2). Indeed, STM inspection of the annealed films revealed a relatively rough surface (Fig. 2a), where a hexagonal lattice of protrusions with a ~ 6 Å periodicity are observed, along with vacancy-type defects and extended areas resembling so-called "biphase" ordered structures, all being well-documented for highly defective Fe_3O_4(111) films and crystal surfaces [23, 24]. Although precise structures were not determined here, we may conclude that iron oxide growth on the *pure* Pt(100) surface leads to the formation of {111}-oriented films. It seems plausible that under these conditions the interface constitutes FeO(111)-like layer, previously found for the monolayer films [22, 25]. Also, our recent study addressing the Pt/Fe_3O_4 interaction [26] showed that charge transfer from an iron oxide to Pt apparently maximizes the number of Pt-Fe contacts at the interface, which will certainly be higher in the case of close-packed, (111) structure. If so, such an FeO(111)-like interfacial layer probably drives the film growth in the (111) direction even on Pt(100). In order to diminish this effect, in the next approach, we employed an Fe buffer layer, first used by Korecki's group for a MgO(001) substrate [15].

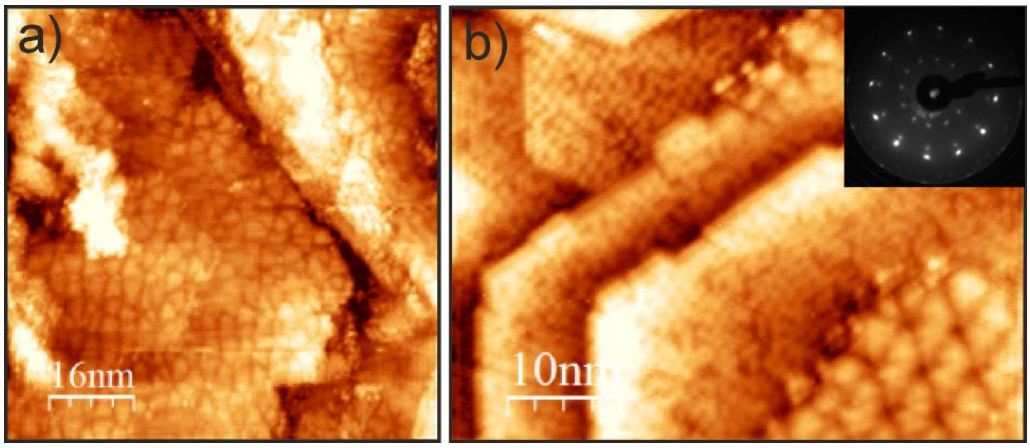

Figure 2. STM images of the films prepared by 25 nm Fe reactive deposition on clean Pt(100) and subsequent annealing in UHV at 645 K for 60 min (a) and then at 775 K (b) for 60 min. Tunnelling conditions: (a) bias = -3 V, current = 0.05 nA; (b) -1 V, 0.1 nA. The inset shows the LEED pattern at 95 eV.

Deposition of a 4 nm thick Fe layer onto the clean Pt(100) surface in UHV leads to lifting of the "hex"-reconstruction. Since Auger spectra showed no Pt signal, the remaining (1×1)

diffraction spots (see Figs. 3a,b) could be assigned to an epitaxially grown Fe(001) layer, as it has only a small mismatch with Pt(100). Subsequent deposition of 4 nm Fe at 300 K in ~5×10^{-6} mbar of O_2 resulted in a diffuse diffraction pattern (Fig. 3c). However, upon prolonged annealing at 775 K, LEED patterns gradually transform into the one well-documented for a $Fe_3O_4(001)$-$(\sqrt{2}\times\sqrt{2})R45^o$ reconstructed surface (Fig. 3d). The diffraction spots become even sharper upon further annealing at 1020 K for 10 min. STM images of the latter sample revealed wide terraces with few screw dislocations (Fig. 4a). The terraces show atomic rows in the [110] direction and anti-phase domain boundaries, all typical of the B-termination. High-resolution images also revealed some vacancy-type defects and ad-species (Figs. 4b,c).

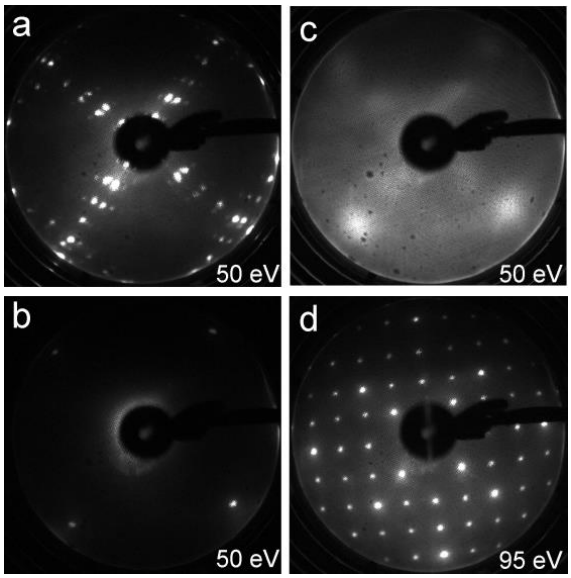

Figure 3. LEED patterns, observed at energies as indicated, for the clean Pt(100)-hex reconstructed surface (a); after deposition of 4 nm-thick Fe layer (b); further reactive deposition of 4 nm Fe in $5x10^{-6}$ mbar of O_2 at 300 K (c); final annealing at 775 K for 100 min (d).

The above preparation was fully reproducible. Note, however, that the sample temperature during iron reactive deposition should be relatively low (300 K in this case), otherwise the metallic Fe layer can, at least partly, be oxidized, and as such the situation becomes very similar to film growth without the Fe buffer layer. Indeed, reactive deposition at 550 K on top of the 4 nm-thick buffer layer led to the mixture of (100) and (111) surfaces (Fig. S1 in Supporting Information). Some increase in oxygen pressure (in the range > 10^{-5}

mbar) sometimes caused formation of small areas characteristic for the FeO(111)/Pt(100) film as judged by LEED (not shown). Nonetheless, the results nicely demonstrate that well-ordered, thin Fe_3O_4(001) films can be grown on a Pt(100) substrate. It is also clear that the presence of a buffer layer several nm thick is necessary for the growth of (001)-oriented films.

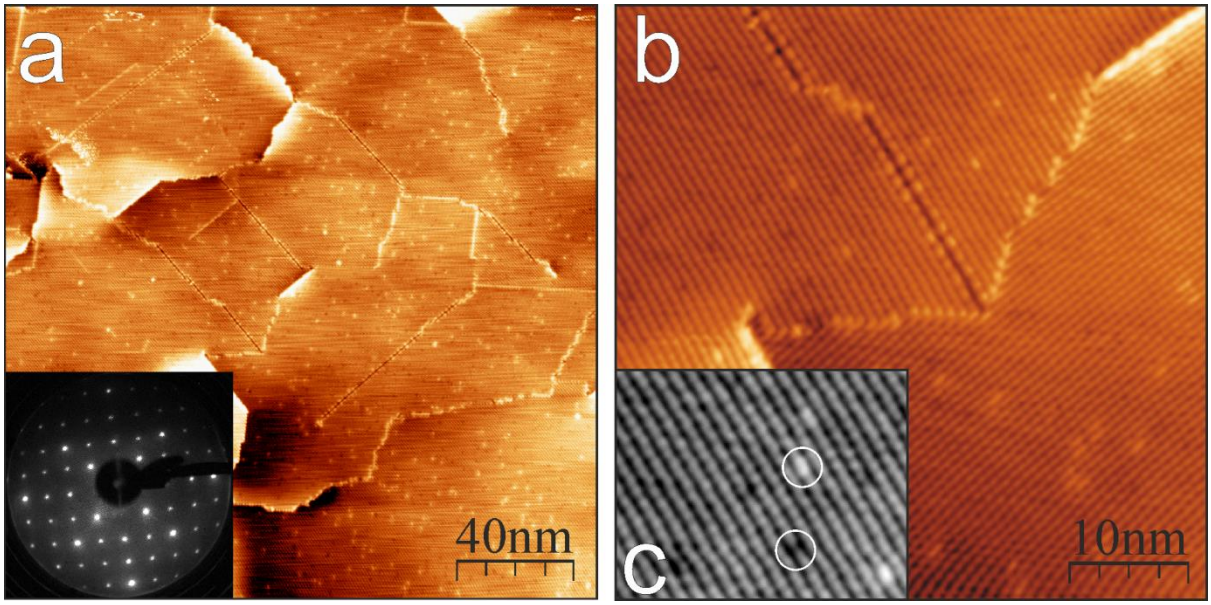

Figure 4. STM images of the Fe_3O_4(001) film on Pt(100) prepared as described in the caption to Fig. 3 after additional UHV-annealing at 1020 K for 10 min. In image (c) (size 30 nm x 24 nm), a vacancy-type defect and an ad-species are highlighted by circles. Tunneling bias = 1.5 V, and current = 4 nA. Inset in panel (a) shows LEED pattern at 95 eV.

To elucidate the role of the Fe buffer layer in the preparation of the (001) films, in the next set of experiments, a much thicker Fe buffer layer (~ 50 nm) was deposited on the Pt(100) surface at 300 K. An oxide film was then formed by reactive Fe deposition at 550 K in 10^{-5} mbar of O_2. The sample was further annealed in UHV at 775 K for ca. 60 min. Although LEED immediately showed an Fe_3O_4(001)-($\sqrt{2}\times\sqrt{2}$)R45^o reconstructed surface, high resolution STM images turned out to be different from those obtained for the sample that had a 4 nm-thick Fe buffer layer. In fact, the images in Fig. 5 are virtually identical to those previously reported for a “dimer”-terminated surface [15]. Since this preparation, in essence, repeats the recipe used by Korecki and coworkers for a MgO(001) substrate, such a similarity in the final structures suggests that the substrate (e.g. MgO(001) and Pt(100)) itself favors solely the

growth of an Fe(001)-like buffer layer which, in turn, governs the growth of a (001)-oriented Fe_3O_4 film. It also appears that the thickness of the buffer layer plays a role in the eventual termination of the film, with the thick layer providing a reservoir of Fe to stabilize an Fe-rich, "dimer" termination. This would imply that Fe atoms have a high mobility within the Fe_3O_4 bulk. In the case of the thin buffer layer, it may be that the buffer layer becomes entirely oxidized, thereby depleting the source of Fe that would otherwise maintain an Fe-rich termination.

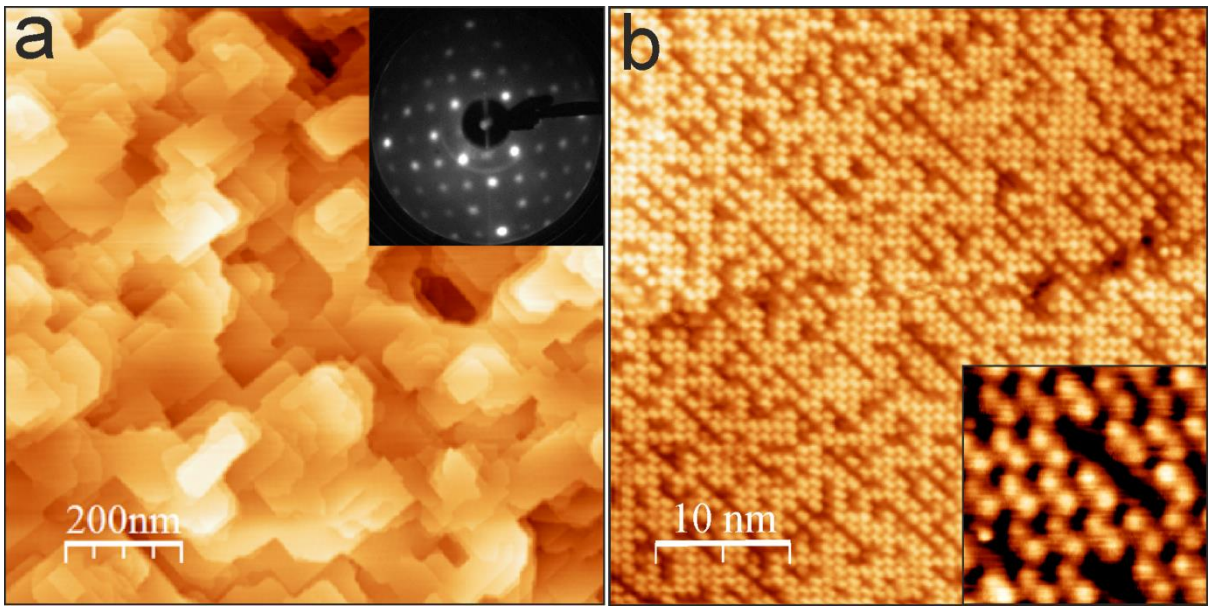

Figure 5. Large scale (a) and high-resolution (b) STM images of the film prepared on 50 nm-thick Fe buffer layer. Tunneling conditions: bias = -3.0 V, current = 0.10 nA; (inset) -1.5 V, 0.10 nA. Inset in panel (a) shows LEED pattern at 95 eV.

To monitor surface transformations of the Fe_3O_4(001) films in more detail, we examined the films prepared with a 4 nm-thick buffer layer using STM and LEED as a function of annealing time at 775 K. The film annealed for 10 min appears to have the "dimer" termination (Fig. 6a) as observed for the preparation of the film with a thick Fe buffer layer (Fig. 5). The structure changed as the sample was annealed for longer periods of time (Fig. 6b), until it became the B-terminated surface after 100 min (Fig. 6c). The corresponding LEED patterns are shown below the images. Annealing of the "as grown" films at higher temperatures, up to 1020 K, accelerates this process, but results in the same, B-terminated

surface. Further oxidation in 10^{-6} mbar of O_2 results in a pristine surface with low defect densities, and this step can be incorporated into the growth procedure.

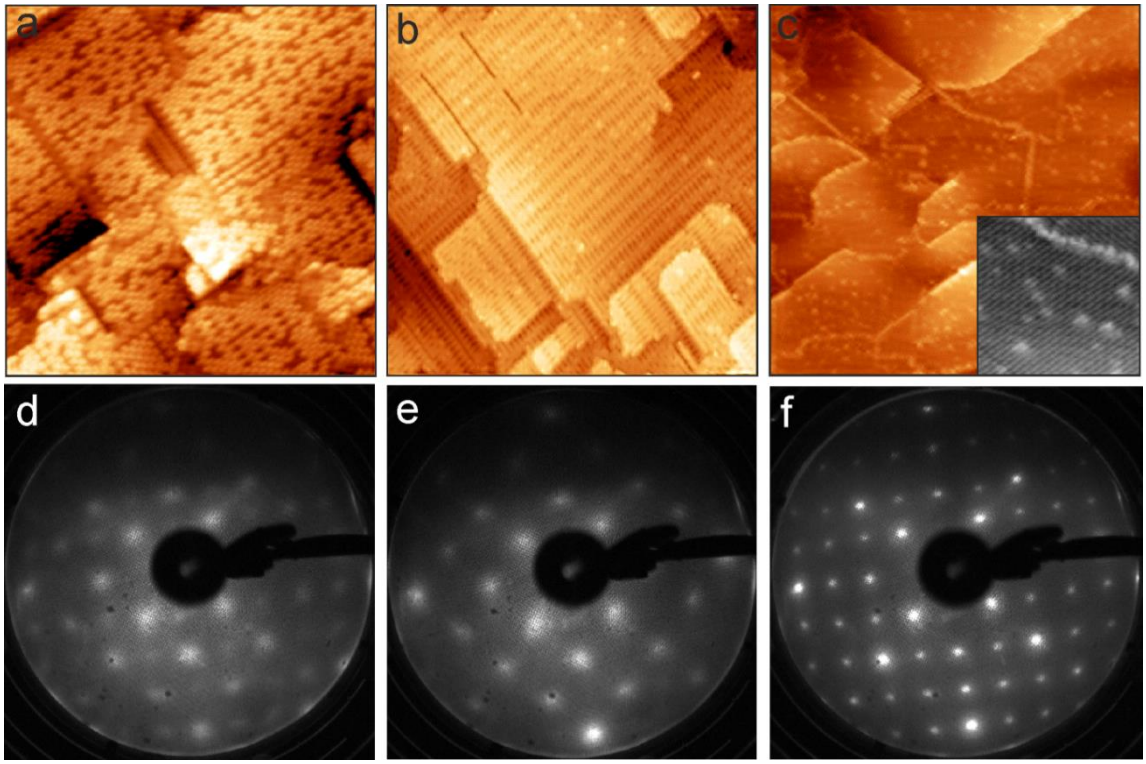

Figure 6. (a-c) STM images and (d-f) corresponding LEED patterns at 95 eV of the Fe_3O_4(001) film grown on 4 nm-thick Fe buffer layer UHV-annealed at 775 K for 10 (a), 60 (b), and 100 (c) min. Image sizes: 50 nm x 50 nm (a,b), 100 nm x 100 nm (c); bias (a,b) = -2 V, (c) = -3 V; current: (a) = 0.1 nA, (b) = 2.0 nA, (c) = 0.64 nA.

We note the similarity of STM images presented in Fig. 6 to those achieved by Novotny et al. [18] by depositing Fe onto a B-terminated surface of a single crystal sample. In particular, we observe that the sample, after 100 minutes of annealing at 775 K, resembles that of the B-terminated surface with 0.025 ML of Fe deposited at 300 K, implying that this surface still has a slight excess of Fe. The termination observed after 60 minutes of annealing bears similarities to the surface seen after 0.8 ML of Fe was deposited on the B-terminated surface and then flashed to 423 K. In the latter case, the termination was assigned by Novotny et al. to pairs of octahedrally coordinated Fe-atoms. This structure differs to the "dimer" model proposed by Korecki et al. [15, 17] regarding the positions of the Fe atoms. Note, however, that Korecki's model is based on STM studies of films grown

on a 20 nm thick Fe buffer layer on MgO(100) at considerably higher temperatures, i.e. 773 K. Therefore, it may well be that these two models are for two different structures.

Figure 6 shows that the Fe-rich, “dimer”-terminated surface transforms into a mixed Fe and O terminated surface upon prolonged annealing. Since the sample annealing was performed in UHV, the transformation indicates diffusion of the surface Fe atoms into the bulk in order to achieve the most stable B-termination, as observed for single crystal samples. The fact that such a transformation was not observed here for the samples with a much thicker buffer layer suggests that it is the buffer layer that supplies Fe to stabilize the otherwise unstable “dimer” termination. (Note that Korecki’s group also observed the “dimer” termination only on films grown on an Fe buffer layer [15]). In the case of the thin buffer layer, this layer may be depleted during annealing, most likely via Fe migration into the Pt crystal bulk. The Fe diffusion across the film may explain the formation of intermediate structures (Fig. 7) which appear to be metastable, as their formation critically depends on the film preparation conditions.

It is still unclear whether the buffer layer is completely oxidized or if metallic Fe remains underneath and/or migrates into the Pt. However, we conclude that the thickness of the Fe buffer layer may be used to control the surface termination.

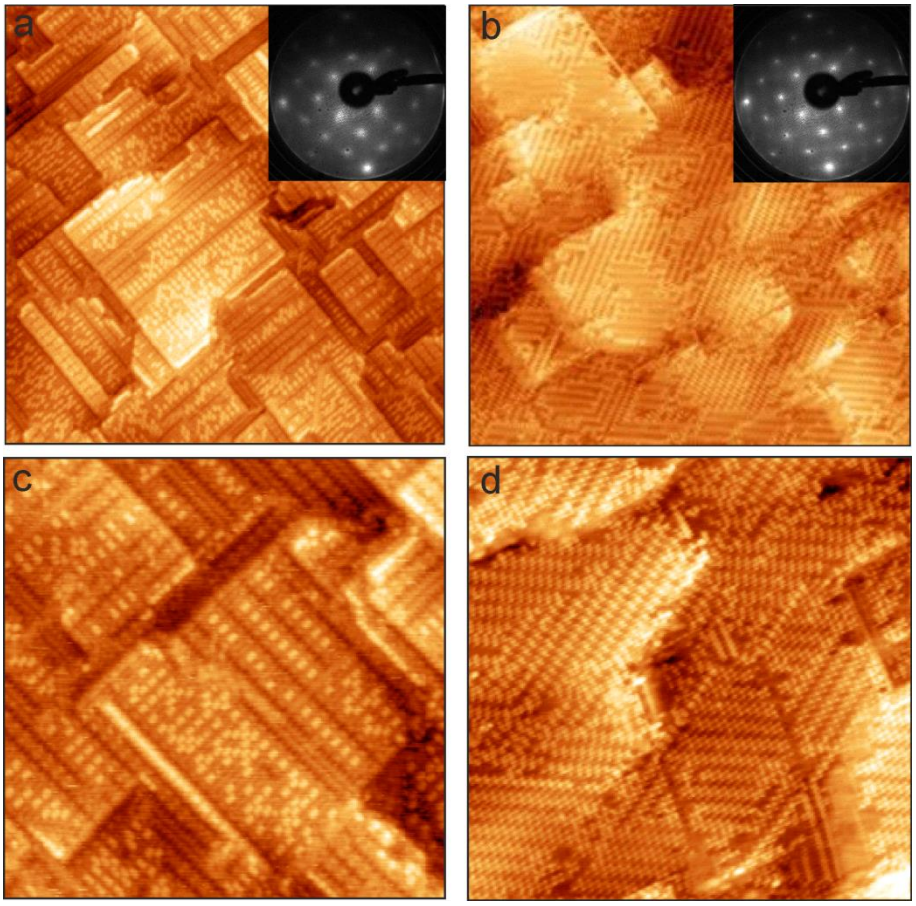

Figure 7. STM images of intermediate surface structures observed on the Fe_3O_4(001) film grown on 4 nm-thick Fe buffer layer UHV-annealed at 775 K for 40 min (a,c) and 70 min (b, d). Image sizes: 100 nm x 100 nm (a,b), and 50 nm x 50 nm (c,d); sample bias = -2 V; current: 2.0 nA (a,c), and sample bias = -1.45 V; current: 0.08 nA (b,d).

4. Conclusions

We have provided a reproducible growth recipe for a Fe_3O_4(001) film on Pt(100) with two stable terminations dependent on growth conditions. These terminations have the same $(\sqrt{2}\times\sqrt{2})R45^{o}$ reconstruction, and can be distinguished only using STM. Growth of both of these terminations requires the presence of a buffer layer to balance the stoichiometry of the film and ensure that it grows epitaxially as the (001) surface. Intermediate terminations were observed during the annealing process for the B-terminated surface, with the surface changing from a dimer-like structure through several Fe-rich surfaces, therefore care must be taken to ensure that the surface has fully transformed into the B-termination. This

process can also be accelerated through the use of higher temperatures, and a surface with very low defect densities can be achieved by annealing in oxygen. With the growth of these thin films, it is now possible to do reactivity studies on these surfaces under well-controlled conditions.

Acknowledgments. The work was supported by German Science Foundation through SFB 1109. The authors acknowledge COST Action CM1104.

References.

[1] H. Kuhlenbeck, S. Shaikhutdinov, H.-J. Freund, Well-Ordered Transition Metal Oxide Layers in Model Catalysis – A Series of Case Studies, Chemical Reviews, 113 (2013) 3986-4034.
[2] S.A. Chambers, Epitaxial growth and properties of thin film oxides, Surface Science Reports, 39 (2000) 105-180.
[3] W. Weiss, W. Ranke, Surface chemistry and catalysis on well-defined epitaxial iron-oxide layers, Progress in Surface Science, 70 (2002) 1-151.
[4] T. Kendelewicz, P. Liu, C.S. Doyle, G.E. Brown Jr, E.J. Nelson, S.A. Chambers, Reaction of water with the (100) and (111) surfaces of Fe3O4, Surface Science, 453 (2000) 32-46.
[5] G.S. Parkinson, Z. Novotný, P. Jacobson, M. Schmid, U. Diebold, Room Temperature Water Splitting at the Surface of Magnetite, Journal of the American Chemical Society, 133 (2011) 12650-12655.
[6] S.F. Ceballos, G. Mariotto, K. Jordan, S. Murphy, C. Seoighe, I.V. Shvets, An atomic scale STM study of the Fe3O4(001) surface, Surface Science, 548 (2004) 106-116.
[7] S.A. Chambers, S. Thevuthasan, S.A. Joyce, Surface structure of MBE-grown Fe3O4(001) by X-ray photoelectron diffraction and scanning tunneling microscopy, Surface Science, 450 (2000) L273-L279.
[8] G. Tarrach, D. Bürgler, T. Schaub, R. Wiesendanger, H.J. Güntherodt, Atomic surface structure of Fe3O4(001) in different preparation stages studied by scanning tunneling microscopy, Surface Science, 285 (1993) 1-14.
[9] B. Stanka, W. Hebenstreit, U. Diebold, S.A. Chambers, Surface reconstruction of Fe3O4(001), Surface Science, 448 (2000) 49-63.
[10] R. Pentcheva, F. Wendler, H.L. Meyerheim, W. Moritz, N. Jedrecy, M. Scheffler, Jahn-Teller Stabilization of a “Polar” Metal Oxide Surface: Fe3O4(001), Physical Review Letters, 94 (2005) 126101.
[11] Z. Łodziana, Surface Verwey Transition in Magnetite, Physical Review Letters, 99 (2007) 206402.
[12] X. Yu, C.-F. Huo, Y.-W. Li, J. Wang, H. Jiao, Fe3O4 surface electronic structures and stability from GGA+U, Surface Science, 606 (2012) 872-879.
[13] G.S. Parkinson, Z. Novotný, P. Jacobson, M. Schmid, U. Diebold, A metastable Fe(A) termination at the Fe3O4(001) surface, Surface Science, 605 (2011) L42-L45.
[14] R. Bliem, E. McDermott, P. Ferstl, M. Setvin, O. Gamba, J. Pavelec, M.A. Schneider, M. Schmid, U. Diebold, P. Blaha, L. Hammer, G.S. Parkinson, Subsurface cation vacancy stabilization of the magnetite (001) surface, Science, 346 (2014) 1215-1218.
[15] N. Spiridis, J. Barbasz, Z. Łodziana, J. Korecki, Fe3O{4}(001) films on Fe(001): Termination and reconstruction of iron-rich surfaces, Physical Review B, 74 (2006) 155423.

[16] J.R. Rustad, E. Wasserman, A.R. Felmy, A molecular dynamics investigation of surface reconstruction on magnetite (001), Surface Science, 432 (1999) L583-L588.
[17] N. Spiridis, E. Madej, J. Korecki, Adsorption of Gold on an Iron-Rich Fe3O4(001) Surface, The Journal of Physical Chemistry C, 118 (2014) 2011-2017.
[18] Z. Novotny, N. Mulakaluri, Z. Edes, M. Schmid, R. Pentcheva, U. Diebold, G. Parkinson, Probing the surface phase diagram of Fe3O4(001) towards the Fe-rich limit: Evidence for progressive reduction of the surface, Physical Review B, 87 (2013) 195410.
[19] M. Fonin, R. Pentcheva, Y. Dedkov, M. Sperlich, D. Vyalikh, M. Scheffler, U. Rüdiger, G. Güntherodt, Surface electronic structure of the Fe3O4(100): Evidence of a half-metal to metal transition, Physical Review B, 72 (2005) 104436.
[20] M. Ritter, H. Over, W. Weiss, Structure of epitaxial iron oxide films grown on Pt(100) determined by low energy electron diffraction, Surface Science, 371 (1997) 245-254.
[21] K. He, L. Zhang, X. Ma, J. Jia, Q. Xue, Z. Qiu, Growth and magnetism of ultrathin Fe films on Pt(100), Physical Review B, 72 (2005) 155432.
[22] S. Shaikhutdinov, M. Ritter, W. Weiss, Hexagonal heterolayers on a square lattice: A combined STM and LEED study of FeO(111) on Pt(100), Physical Review B - Condensed Matter and Materials Physics, 62 (2000) 7535-7541.
[23] N.G. Condon, F.M. Leibsle, T. Parker, A.R. Lennie, D.J. Vaughan, G. Thornton, Biphase ordering on Fe3O4(111), Physical Review B - Condensed Matter and Materials Physics, 55 (1997) 15885-15894.
[24] S.K. Shaikhutdinov, M. Ritter, X.G. Wang, H. Over, W. Weiss, Defect structures on epitaxial Fe 3O 4(111) films, Physical Review B - Condensed Matter and Materials Physics, 60 (1999) 11062-11069.
[25] G.H. Vurens, V. Maurice, M. Salmeron, G.A. Somorjai, Growth, structure and chemical properties of FeO overlayers on Pt(100) and Pt(111), Surface Science, 268 (1992) 170-178.
[26] M.G. Willinger, W. Zhang, O. Bondarchuk, S. Shaikhutdinov, H.-J. Freund, R. Schlögl, A Case of Strong Metal–Support Interactions: Combining Advanced Microscopy and Model Systems to Elucidate the Atomic Structure of Interfaces, Angewandte Chemie International Edition, 53 (2014) 5998-6001.